HHS Public Access

Author manuscript

Biochemistry. Author manuscript; available in PMC 2021 February 06.

Published in final edited form as:

Biochemistry. 2020 July 28; 59(29): 2698–2706. doi:10.1021/acs.biochem.0c00485.

Activation Loop Dynamics Are Coupled to Core Motions in Extracellular Signal-Regulated Kinase-2

Dylan B. Iverson,
Department of Biochemistry, University of Colorado at Boulder, Boulder, Colorado 80309, United States

Yao Xiao,
Department of Biochemistry, University of Colorado at Boulder, Boulder, Colorado 80309, United States

David N. Jones,
Department of Pharmacology, University of Colorado Denver Anschutz Medical Campus, Aurora, Colorado 80045, United States

Elan Z. Eisenmesser,
Department of Biochemistry and Molecular Genetics, University of Colorado Denver Anschutz Medical Campus, Aurora, Colorado 80045, United States

Natalie G. Ahn
Department of Biochemistry, University of Colorado at Boulder, Boulder, Colorado 80309, United States

Abstract

The activation loop segment in protein kinases is a common site for regulatory phosphorylation. In extracellular signal-regulated kinase 2 (ERK2), dual phosphorylation and conformational rearrangement of the activation loop accompany enzyme activation. X-ray structures show the active conformation to be stabilized by multiple ion pair interactions between phosphorylated threonine and tyrosine residues in the loop and six arginine residues in the kinase core. Despite the extensive salt bridge network, nuclear magnetic resonance Carr–Purcell–Meiboom–Gill relaxation

Corresponding Author: Phone: (303) 492-4799; natalie.ahn@colorado.edu.

Complete contact information is available at: https://pubs.acs.org/10.1021/acs.biochem.0c00485

ASSOCIATED CONTENT

Supporting Information

The Supporting Information is available free of charge at https://pubs.acs.org/doi/10.1021/acs.biochem.0c00485.

Detailed Materials and Methods, residues that participate in the global conformational exchange process that are distributed throughout the kinase core (Figure S1), assignments of NMR resonances for activation loop residues L182 and V186 (Figure S2), activation loop residue assignments in 2P-ERK2 that are confirmed by NOE through-space interactions (Figure S3), methyl peaks that reveal changes in conformational exchange of core residues by activation loop mutations (Figure S4), CPMG relaxation–dispersion plots that report changes in conformational exchange of core residues by activation loop mutations (Figure S5), suppression of R_{ex} by mutation L182I in 2P-ERK2 (Figure S6), exchange parameters for [*methyl*-^{13}C]ILV probes in WT 0P- and 2P-ERK2 (Table S1), exchange parameters for [*methyl*-^{13}C]ILV probes in mutant ME/GG 0P-ERK2 (Table S2), and exchange parameters for [*methyl*-^{13}C]ILV probes in mutants L182I and V186I, 0P- and 2P-ERK2 (Table S3) (PDF)

Accession Codes

ERK2, P28482; MKK1, Q02750.

The authors declare no competing financial interest.

dispersion experiments show that the phosphorylated activation loop is conformationally mobile on a microsecond to millisecond time scale. The dynamics of the loop match those of previously reported global exchange within the kinase core region and surrounding the catalytic site that have been found to facilitate productive nucleotide binding. Mutations in the core region that alter these global motions also alter the dynamics of the activation loop. Conversely, mutations in the activation loop perturb the global exchange within the kinase core. Together, these findings provide evidence for coupling between motions in the activation loop and those surrounding the catalytic site in the active state of the kinase. Thus, the activation loop segment in dual-phosphorylated ERK2 is not held statically in the active X-ray conformation but instead undergoes exchange between conformers separated by a small energetic barrier, serving as part of a dynamic allosteric network controlling nucleotide binding and catalytic function.

Graphical Abstract

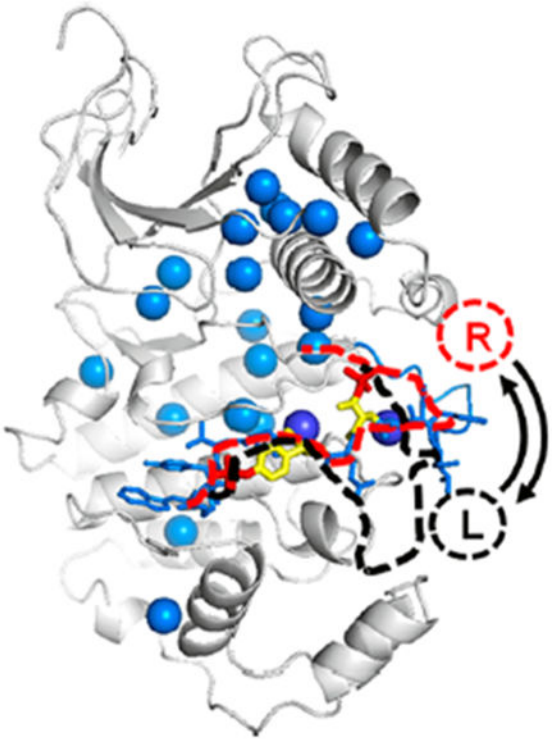

Extracellular-regulated kinases 1 and 2 (ERK1/2) are key enzymes in the MAP kinase signal transduction pathway, regulated upstream by the protein kinases, A-, B-, and C-Raf, and MAP kinase kinases 1 and 2 (MKK1/2, also known as MEK1/2).[1] In mammalian cells, the Raf/MKK/ERK pathway controls cell proliferation, survival, and cell motility.[2] In disease states such as cancer, elevated pathway flux underlies tumor growth, metastasis, and other hallmarks of malignancy.[3,4] Oncogenic B-RAF-V600E/K mutations lead to increased levels of activation of MKK1/2 and ERK1/2, and market-approved inhibitors toward B-RAF-V600E/K and MKK1/2 are first-line treatments for metastatic melanomas harboring these mutations.[5] However, tumor adaptation invariably leads to resistance through pathway reactivation.[6] Although ERK inhibitors have been shown to be effective toward tumor cells

and xenografts resistant to B-RAF and MKK inhibitors,[7–10] none have yet succeeded in clinical trials. Thus, a deeper mechanistic understanding of ERK activation is needed to develop therapeutics toward this target.

Crystallographic studies show obvious structural differences between inactive, unphosphorylated (0P) and active, dual-phosphorylated (2P) ERK2; these occur at the activation loop segment, where the two sites of regulatory phosphorylation reside (Figure 1).[11,12] Remodeling of the activation loop results in extensive salt bridge interactions between the negatively charged phosphoryl groups on pT183 and pY185 and multiple Arg residues in the N- and C-terminal lobes. By contrast, large structural changes are absent within the kinase core, surrounding the nucleotide binding pocket and active site. This differs from other kinase family members, where activation loop phosphorylation is accompanied by repositioning of key residues that are important for catalysis, including a conserved DFG motif that coordinates metal in Mg^{2+}ATP; a conserved salt bridge between Lys52 (strand β3) and Glu69 (helix αC) residues that coordinates phosphoryl groups in ATP; and hydrophobic residues in R- and C-spine structural elements throughout the kinase core.[13,14] In ERK2, the catalytic site residues are largely overlapping between 0P and 2P states, and structural differences accompanying activation are hard to detect within the kinase core.[11,12]

Nevertheless, solution studies of ERK2 have revealed significant changes in protein dynamics upon activation. Nuclear magnetic resonance (NMR) Carr–Purcell–Meiboom–Gill (CPMG) relaxation dispersion (RD) experiments of [*methyl*-^{13}C]Ile/Leu/Val (ILV) residues reveal changes in chemical exchange rate constants (k_{ex}) following dual phosphorylation of ERK2, leading to correlations among 19 ILV residues throughout the core of the active kinase that can be fit globally (Figure 1).[15,16] The global exchange behavior in 2P-ERK2 is consistent with interconversion between two dominant conformational states;[17,18] this is supported by shifts in populations upon inhibitor binding, described below. The simplest model involves a dominant “L” state conformation in 0P-ERK2, which in 2P-ERK2 shifts toward a new “R” state in equilibrium exchange with the L state on a microsecond to millisecond time scale.[15] The conformational differences between L and R states have not been fully elucidated. Within the active site, X-ray structures of 0P- and 2P-ERK2 apoenzymes look nearly identical. However, co-crystal structures reveal a distorted, nonproductive interaction with the bound nucleotide in 0P-ERK2, in contrast to a productive binding mode in 2P-ERK2.[19,20] Correspondingly, hydrogen exchange mass spectrometry (HX-MS) measurements reveal changes in conformational mobility within the active site upon activation and ligand binding. [ISP check][20–22] Together, the evidence has led us to propose that motions within the active site promote catalytic competency by enabling small changes in nucleotide binding interactions.

The role of the activation loop in L $\rightleftharpoons$ R exchange is still incompletely understood. NMR and HX-MS experiments have suggested that motions in the activation loop might couple to the global exchange behavior within the kinase core. This was proposed on the basis of the ability of tight binding inhibitors to induce shifts in populations of L and R conformers.[20,23] Thus, whereas NMR measurements show an L:R ratio of ≈20:80 in the apo state of 2P-ERK2, binding of the ERK inhibitor, Vertex-11e, shifts the L $\rightleftharpoons$ R exchange completely toward R, while binding of the inhibitor, SCH772984, shifts the exchange completely toward

L. These shifts occur even though structural differences between bound and apo forms are hard to detect by X-ray crystallography, suggesting that they involve changes in protein mobility around similar average conformations.[20] By HX-MS, these two inhibitors induce opposite effects within the P + 1 substrate recognition motif located adjacent to the activation loop, and kinetic measurements show that they decrease or increase the rate of pT183 and pY185 dephosphorylation by MAP kinase phosphatase.[20] These findings suggested that inhibitors with properties of conformational selection might modulate motions in both the kinase core and the activation loop of 2P-ERK2. This was unexpected, on the basis of the salt bridge network formed between phosphorylated activation loop and core Arg residues, which were predicted to form a stable structure.[12,24] Therefore, additional studies are needed to investigate whether the L $\rightleftharpoons$ R exchange involves coupling between motions in the phosphorylated activation loop and within the kinase core.

Here we use NMR CPMG relaxation dispersion measurements to monitor exchange dynamics of the activation loop in ERK2. Examination of wild-type (WT) 2P-ERK2 reveals that motions of the activation loop are indeed correlated with the global exchange behavior of the kinase core. Mutations in the hinge region between the N- and C-terminal domains, which had been previously shown to induce a partial shift toward the R state in the 0P form of ERK2, induced a corresponding change at the activation loop. Conversely, mutations at the activation loop alter the patterns of global exchange in the core. Taken together, the findings reveal that the phosphorylated activation loop of ERK2 undergoes dynamics on a microsecond to millisecond time scale, and that the motions at the activation loop are coupled to the global motions within the core and active site that accompany catalytic activation.

MATERIALS AND METHODS

Detailed methods are provided in the Supporting Information.

Protein Preparation.

L182A, L182I, V186A, V186I, and M106G/E107G (“ME/GG”) substitutions were introduced by site-directed mutagenesis of rat His_6-ERK2 in the pET23a plasmid, and [*methyl*-^{13}C]ILV-labeled samples of 0P-ERK2 were expressed in *Escherichia coli,* following methods previously described.[15,25,26] Proteins were then purified from cell lysates by Ni^{2+}-NTA chromatography (Bio-Rad), followed by HiTrapQ and Sephacryl S200 chromatography (GE Healthcare) as described previously.[15,25] 2P-ERK2 was prepared from 0P-ERK2 purified through HiTrapQ, by phosphorylation *in vitro* with constitutively active MKK1-(ΔN4/S218D/M219D/N221D/S222D)[27,28] and further purification by Sephadex S200 chromatography. Proteins were concentrated to 03–0.4 mM and exchanged into NMR buffer [50 mM Tris (pH 7.4), 150 mM NaCl, 5 mM $MgSO_4$, 0.1 mM EDTA, 5 mM dithiothreitol, and 2.5% glycerol, in 100% D_2O] for NMR experiments. Phosphorylation stoichiometries quantified by mass spectrometry[29] measured <1% mono-phosphorylated pY185 in 0P-ERK2 and >95% dual-phosphory-lated pT183/pY185 in 2P-ERK2.

NMR Spectroscopy.

NMR CPMG experiments for WT ERK2 were collected at 600, 800, and 900 MHz, and data for ERK2-ME/GG were collected at 800 and 900 MHz as described, all at 25 °C.[15,25] Two-dimensional (2D) (^{13}C, ^{1}H) methyl HMQC experiments for L182A/I and V186A/I ERK2 were performed at 900 MHz and 25 °C using a Varian 900 MHz Direct Drive NMR system with a z-axis cryoprobe, measuring between 128 and 192 complex points in ^{13}C with a spectral width of 21 ppm (4800 Hz) and 1024 complex points in ^{1}H with a spectral width of 13 ppm (12000 Hz). Three-dimensional (3D) (^{13}C, ^{13}C, ^{1}H) NOESY experiments were performed on the [*methyl*-^{13}C]ILV-labeled ERK2 samples using a 350 ms mixing time. Experiments were acquired with 54 and 52 complex points (15.9 and 15.3 ms, respectively) in the t_1(^{13}C) and t_2(^{13}C) dimensions, respectively, and 1024 complex points in the acquisition period. Constant time Carr–Purcell–Meiboom–Gill relaxation–dispersion experiments were performed on WT and mutant samples of 0P- and 2P-ERK2. CPMG data series were collected with τ values of 5–0.25 ms where $\nu_{CPMG} = 1/4\tau$, and 2τ is the time interval between successive 180° ^{13}C refocusing pulses.

Data Analysis.

Data were processed using the NMRPipe software package.[30] A majority of peaks in the spectra of wild-type 0P- and 2P-ERK2 were previously assigned as described previously.[25] Additional peaks were assigned to residues L182 and V186 by comparing 2D (^{13}C, ^{1}H) methyl-optimized HMQC spectra of WT-ERK2 to L182A, L182I, V186A, and V186I mutants in their unphosphorylated and dual-phosphorylated forms and observing peak disappearance. Where possible, peak assignments were verified using through-space interactions detected in 3D (^{13}C, ^{13}C, ^{1}H) HMQC-NOESY spectra.

2D methyl HMQC and 3D (^{13}C, ^{13}C, ^{1}H) HMQC-NOESY were analyzed using the CCPNMR software package.[31,32] For calculation of R_2 for CPMG experiments, peak intensities were analyzed using FuDA[33] (http://pound.med.utoronto.ca/software). The effective signal relaxation rate, $R_{2,\text{eff}}$, was calculated by the equation $R_{2,\text{eff}} = -1/T \ln[I(\nu_{CPMG})/I(0)]$, where T is the constant time relaxation period and $I(\nu_{CPMG})$ and $I(0)$ are peak intensities recorded with and without a CPMG relaxation period, respectively. To quantify exchange dynamics, a two-state exchange model was applied using nonlinear least-squares fitting to the generalized Carver–Richards equation using CATIA[34,35] (http://pound.med.utoronto.ca/software). Fitting generally yielded exchange rate constants ($k_{ex} = k_{AB} + k_{BA}$, populations (p_A and p_B), and ^{13}C chemical shift changes (in parts per million) between states A and B ($|\Delta\delta_{CPMG}$ ^{13}C|, assuming $\Delta|\delta_{CPMG}$ ^{1}H| = 0). For group (global) fits, values of k_{ex} and p_B were forced to be the same for all included methyls. Where p_B could not be determined with confidence, a simplified, fast exchange limit equation

$$R_{2,\text{eff}} = R_{2,0} + \frac{p_A p_B \Delta\omega_{AB}^2}{k_{ex}}\left[1 - \frac{2\tanh\left(\frac{k_{ex}\tau_{CP}}{2}\right)}{k_{ex}\tau_{CP}}\right]$$

was used to estimate k_{ex} and the term $p_A p_B \Delta\omega_{AB}^2$. $R_{2,0}$ is the basal transverse relaxation rate; τ_{CP} is the interval between 180° ^{13}C refocusing pulses, and $\Delta\omega_{AB}$ is the difference in chemical shift between the two exchanging states.

A jackknifing method was used to evaluate the consistency of CPMG global fits.[36] For global fits consisting of N unique methyls, a random number generator was used to create 50 random subsets of $N-4$, $N-6$, and $N-9$ residues. These subsets were then individually fit using CATIA, each generating global values for k_{ex} and p_B. For a global motion, the error (standard deviation) would be expected to be relatively low; that is, results should be independent of which residues were selected.

RESULTS

NMR Resonance Assignments.

To monitor motions of the activation loop, experiments were conducted to assign resonances corresponding to residues L182 and V186, which are located next to the two phosphorylation sites, T183 and Y185 (Figure 1). L182 and V186 were individually mutated to Ala or Ile, and mutant proteins were selectively labeled with [*methyl*-^{13}C]ILV as described previously.[15,25] The resulting 2D (^{13}C, ^{1}H) methyl heteronuclear multiple-quantum coherence (HMQC) spectra were well resolved for both 0P and 2P forms of ERK2 (Figure S1A,B). Clear and consistent peaks present in WT ERK2 systematically disappeared with each residue mutation (Figure S2A,B), which allowed for identification of their resonances. The chemical shifts of L182 and V186 in WT-ERK2 varied dramatically between the 0P- and 2P-kinase forms (Figure S1B), which can be attributed to their different chemical environments in the absence or presence of negatively charged phosphoryl groups.

To verify the assignments for L182 and V186, 3D CCH-NOESY spectra were recorded and analyzed. On the basis of the X-ray structure of 2P-ERK2 (Protein Data Bank entry 2ERK), potential through-space NOE interactions were predicted between L182 and V186, and between these residues and L144, L168, 1196, and 1207 (Figure S3A). In accordance, residues within this cluster were mapped in WT 2P-ERK2 (Figure S3B). NOE cross-peaks were observed for all six residues, providing substantial validation of their assignments. Similarly, the mutant 2P-ERK2-L182I showed NOE cross-peaks connecting V186 to L168, L144, and I196, while a resonance assigned to I182 showed no cross-peaks, most likely due to its weak intensity (Figure S3C). Although the X-ray structure of WT 0P-ERK2 (Protein Data Bank entry 5UMO) suggested proximity between residue pairs L182-L232 and V186-L168, NOE cross-peaks between these residues were not detectable, suggesting increased dynamics in solution relative to the crystal (Figure S3D).

Dynamics of the Activation Loop.

The Carr–Purcell–Meiboom–Gill relaxation dispersion (CPMG-RD) experiment measures motions in proteins on microsecond to millisecond time scales by probing the effect of conformational exchange upon the rate of transverse (spin–lattice) relaxation (R_2).[17] In a two-state chemical exchange system, an ILV methyl group will experience two distinct chemical environments, resulting in interconversion between states A and B, with chemical

exchange rate constant ($k_{ex} = k_{AB} + k_{BA}$), and time-sampled population averages for the two states (p_A and p_B). The exchange results in a more rapid R_2. Higher refocusing frequencies (ν_{CPMG}) increasingly mitigate the exchange contribution to transverse relaxation (R_{ex}). Mathematical models of exchange, including the Carver—Richards formulation, can then be employed to extract values for k_{ex}, p_A, and p_B.

In previous CPMG-RD measurements, [*methyl*-^{13}C]ILV residues throughout 0P-ERK2 showed either uncorrelated k_{ex} (~100–2500 s^{-1}) or no detectable exchange within the CPMG time scale (Figure 2A). Strikingly, 19 methyls located throughout the kinase core in 2P-ERK2 converged to lower k_{ex} values and could be fit globally to yield the following parameters: $k_{ex} \approx 320 \pm 17\ s^{-1}$, $p_A \approx 83 \pm 0.5\%$, and $p_B \approx 17 \pm 0.5\%$ (Figure 2B and ref 15). We therefore asked if the newly assigned residues, L182 and V186, also showed chemical exchange consistent with the global fit. Like other residues that were included in the global motion, L182 and V186 both showed reduced k_{ex} and increased R_{ex} values in 2P-ERK2 compared to 0P-ERK2 (Figure 2A,B). Furthermore, both residues could be included in the global fit with the previous 19 residues without altering the quality of the fitting, to yield the following values: $k_{ex} = 310 \pm 16\ s^{-1}$, $p_A = 83 \pm 0.5\%$, and $p_B = 17 \pm 0.5\%$ (Table S1). From these parameters, global motions on a millisecond time scale ($k_{A,B} = 53\ s^{-1}$; $k_{B,A} = 260\ s^{-1}$) were estimated. By contrast, global fitting attempts failed to converge for 0P-ERK2 (Table S1). The results provide evidence that the distribution of motions in 2P-ERK2 is more compressed than 0P-ERK2 and reveals a globally coupled dynamic that includes the phosphorylated activation loop in addition to the active site.

Coupling of Exchange between the Kinase Core and the Activation Loop.

We asked if mutations within the core of ERK2 that are known to perturb global exchange might also alter the exchange properties of the activation loop. Previous CPMG analyses showed that the $M_{106}E_{107} \rightarrow G_{106}G_{107}$ mutation ("ME/GG"), located at the hinge region between the N- and C-terminal domains, induced a global exchange process even in the unphosphorylated form of the kinase.[15] Furthermore, kinetic measurements showed that the ERK2-ME/GG mutant could be activated by phosphorylation of T183 and the mutation of Y185E, to levels comparable to its dual-phosphorylated form.[37] Thus, ME/GG enables kinase activation by a single phosphorylated residue, bypassing the need for the dual phosphorylation normally required for WT ERK2 activation. We therefore examined the effect of the ME/GG mutation on chemical exchange at the activation loop. V186, and to a lesser extent L182, showed an increased R_{ex} in mutant 0P-ERK2-ME/GG compared to WT 0P-ERK2 (Figure 2C). Both residues appear to exchange similarly with the remaining core ILV methyls in ERK2-ME/GG, with a global fit yielding the following values: $k_{ex} = 1300 \pm 150\ s^{-1}$, $p_A = 90 \pm 20\%$, and $p_B = 10 \pm 20\%$ (Table S2A). The statistical significances of the global fit values were confirmed using a jackknife protocol (Table S2B). The effects of the ME/GG mutation on the dynamics of the activation loop residues are consistent with coupling between motions at the activation loop and the global exchange behavior within the kinase core.

Conversely, we asked if mutational perturbations at the activation loop could alter the global exchange behavior of residues within the kinase core. Previous analyses of WT 2P-ERK2

showed that the p_A:p_B population ratio could be estimated from HMQC spectra for methyls whose chemical shift differences between R and L were larger than the chemical exchange rate constant (i.e., $\Delta\omega \gg k_{ex}$).[15] As this defines a slow chemical exchange, each methyl appeared as two peaks in 2P-ERK2, corresponding to ~80% R and ~20% L states (Figure 3A and Figure S4A, red). By comparison, the same methyls appeared as single peaks in 0P-ERK2, which overlapped with the minor state in 2P-ERK2, thus reflecting a conformational shift toward nearly 100% L (Figure 3A and Figure S4A, black). Mutation of either L182 or V186 to Ala resulted in a substantial shift in the population of each core residue in 2P-ERK2, to match that in 0P-ERK2 (Figure 3B,C and Figure S4B,C). This shows that Ala mutations at the activation loop interfere with the shift to the R state normally observed in WT 2P-ERK2.

Next, conservative mutations substituting L182 or V186 with Ile were examined (Figure 3D,E and Figure S4D,E). As in WT ERK2, HMQC peaks corresponding to core ILV methyls in ERK2-V186I appeared largely in the L state in the unphosphorylated kinase and shifted toward the R state following dual phosphorylation (Figure 3E and Figure S4E). By contrast, ERK2-L182I showed mixed effects. Most core methyls responded similarly to WT, with chemical shifts indicating a predominant R state in 2P-ERK2 [e.g., I72, I87, I131, and I345 (Figure 3D and Figure S4D)]. However, some residues showed variations in chemical shifts in 2P-ERK2-L182I [e.g., I82, I138, and I241 (Figure 3D and Figure S4D)], suggesting regional perturbations to a distinct state.

Follow-up studies were conducted to examine the L182A, L182I, and V186A mutants by NMR CPMG. In each case, clear trends in R_{ex} were observed from CPMG-RD curves (Figure 4 and Figure S5). In the 2P form of mutant L182A, R_{ex} was substantially repressed compared to that of WT 2P-ERK2 (Figure 4A,B and Figure S5A,B). This is consistent with an inability of the mutant to form the R state, as also indicated by chemical shifts in HMQC spectra (Figure 3A,B and Figure S4A,B). Importantly, R_{ex} also systematically decreased in the dual-phosphorylated L182I mutant compared to that of the WT kinase (Figure 4A,C and Figure S5A,C), although to a lesser degree than in L182A Thus, chemical exchange throughout the core was suppressed by the L182I mutation (Figure S6A). In the 2P V186I mutant, R_{ex} values were mostly comparable to that of the WT kinase (Figure 4A,D and Figure S5A,D), with a few exceptions (Figure S6B). Individual fits of data collected at 900 MHz showed significant errors for k_{ex}, p_A and p_B (Table S3A,B). Therefore, jackknife protocols were carried out to test significance, yielding k_{ex} = 1600 ± 210 s^{-1}, p_A = 93 ± 3%, and p_B = 7 ± 3% for 2P-ERK2-L182I and k_{ex} = 1100 ± 190 s^{-1}, p_A = 92 ± 2%, and p_B = 8 ± 2% for 2P-ERK2-V186I (Table S3C). Overall, both phosphorylated forms of the L182I and V186I mutants largely retained the global exchange behavior of the WT 2P enzyme. In the unphosphorylated forms of L182I and V186I, R_{ex} values were uniformly low, as in WT 0P-ERK2 (Figure 4 and Figure S6). The reciprocal interactions between the core and the activation loop help confirm findings from CPMG analyses of WT ERK2 indicating that the activation loop undergoes slow motions that are coupled to allosteric motions within the kinase core.

DISCUSSION

Our study demonstrates that the dual-phosphorylated activation loop of ERK2 undergoes motions, and that these are coupled to residues within the kinase core. This is shown by correlations between NMR CPMG measurements of activation loop residue probes and the globally fitted values of k_{ex}, p_A, and p_B for core residue methyl groups. Mutational studies further validate this model for coupling, based on reciprocal interactions between the kinase core and the activation loop. Specifically, the ME/GG mutation lowers the energy barrier to allow a partial shift toward the R state in 0P-ERK2 and correspondingly enables a partial shift in the activation loop. Conversely, mutations of activation loop residues L182 and V186 to Ala interfere with the ability of phosphorylated ERK2 to form the R state, while mutations to Ile alter exchange parameter values but retain their correlations with methyls within the core. The significance of global exchange occurring within the kinase core is its link to catalytic activation, where formation of the R state in 2P-ERK2 accompanies a catalytically productive binding mode for the nucleotide, observed by X-ray crystallography and HDX-MS.[20] Transmission of dynamic changes between the kinase core and the activation loop reveals a conformational coupling model that expands our understanding of global exchange and allosteric regulation of ERK2.

The ability of the phosphorylated activation loop to undergo motions was unexpected, given X-ray structures showing extensive salt bridging between pT183/pY185 and six Arg residues in the N- and C-terminal lobes.[12] These salt bridges potentially explain why the relatively incoherent motions within 0P-ERK2 become more tightly correlated in 2P-ERK2. The estimated L:R ratio of ≈20:80 at 25 °C corresponds to a small free energy difference $\Delta G^\circ_{L\rightarrow R}$ of approximately −0.8 kcal/mol. Therefore, to the extent that a large conformational change at the activation loop dominates the energetics of the L ⇌ R exchange, the phosphate salt bridges appear to contribute relatively little energetic stabilization. Temperature-dependent shifts in peak intensities for probes of L ⇌ R exchange within the kinase core yield the following estimates: $\Delta H^\circ_{L\rightarrow R}$ = +9.7 ± 1.1 kcal/mol, and $\Delta S^\circ_{L\rightarrow R}$ = +36 ± 2 cal mol^{-1} deg^{-1}.[15] Such values are consistent with an unfavorable enthalpy change upon formation of surface-exposed salt bridges, offset by a favorable entropic contribution from solvent. As a result, the energetic difference is small between the unphosphorylated and dual-phosphorylated conformations. This may enable mobility of the phosphorylated activation loop, despite extensive charge–phosphate interactions.

Several studies have documented motions in unphosphorylated kinase activation loops. Experimentally, motions in the activation loop have been observed in unphosphorylated Src by NMR relaxation, and in unphosphorylated p38α MAPK by site-directed spin labeling EPR.[38,39] These are supported by molecular dynamics (MD) simulations, e.g., with Src family kinases, p38α MAPK and Wnk1, which show conformational equilibria between inactive and active state populations on microsecond time scales.[40–43] However, the evidence so far that activation loop segments undergo motions after conversion to their phosphorylated forms has been limited. For example, MD analyses of Src and Wnk1 suggest that phosphorylation locks the activation loop in an extended conformation that appears immobile on the simulation time scale, even with enhanced sampling methods.

Molecular dynamics simulations may not be able to detect motions of kinase activation loops, due to insufficient sampling. For example, the activation loop motions revealed by our study were not apparent in 1 μs MD simulations of 0P- or 2P-ERK2.[44] Therefore, experimental approaches capable of sampling slower motions are needed to fully address the stability of activation loops following phosphorylation. In 2P-p38α MAP kinase, ^{15}N CPMG-RD revealed slow motions of the activation loop coupled to global exchange after binding to a docking motif peptide ligand.[45] Recent studies of Aurora A showed changes in time-resolved Förster resonance energy transfer measurements of sensors in the activation loop and conserved DFG motif; these tracked conformational transitions corresponding to activation loop remodeling coupled to DFG in $\rightleftharpoons$ out motions.[46,47] A panel of inhibitors displayed variable selections for distinct conformational states.[46] Together, these findings suggested that in its phosphorylated form, Aurora A undergoes conformational transitions at its activation loop, driven by the binding energy for the inhibitor. Although WT ERK2 does not appear to undergo similar switching between DFG in and DFG out conformers, two tight binding inhibitors, Vertex-11e and SCH772984, do show conformational selection for R and L states, respectively. Thus, both ERK2 and Aurora A show similar behavior, in that tight binding inhibitors can induce conformational transitions at the activation loop following binding to the active site.[20,23] Conceivably, the ability of phosphorylation to couple motions at the activation loop with motions within the core may be shared by many protein kinases. To the degree that the exchange behavior in 2P-ERK2 involves disruption of multiple phosphate salt bridges, protein kinases activated by one phosphorylation event might also undergo activation loop motions on microsecond to millisecond time scales.

Our finding that the activation loop can be subject to conformational exchange suggests new regulatory mechanisms for ERK2. Functional effects of coupling have been shown by the ability of Vertex-11e and SCH772984 to inhibit or activate dephosphorylation of 2P-ERK2 by the MAP kinase phosphatase, MKP3/DUSP6.[20] Thus, activation loop motions allow active site ligands to alter the L $\rightleftharpoons$ R equilibrium and control the accessibility of the activation loop residues to phosphatase. Potentially, this may impact the recognition of substrates interacting with residues in the P + 1 region or the adjacent DEF docking motif binding site.[48] Conversely, the coupling behavior predicts that proteins or substrates that interact with the loop might control the dynamics in the active site of ERK2, with a potential impact on steps in enzyme turnover. Future studies are needed to investigate the mechanism for coupling and to investigate the role of loop dynamics on intermediate steps in catalysis.

Supplementary Material

Refer to Web version on PubMed Central for supplementary material.

ACKNOWLEDGMENTS

The authors are indebted to Maria Hoh and Thomas Lee for help with mass spectrometry analyses and to Laurel Pegram for critical reading of the manuscript.

Funding

This work was supported by National Institutes of Health (NIH) Grants R01GM114594 and R35GM136392 (N.G.A.), NIH Grant R56CA230069 and National Science Foundation Grant 1807326 (E.Z.E.), NIH Grant R01AI121253 (D.N.J.), NIH Grant T32GM008759 (D.B.I.), and NIH Grants S10RR026641 and S10OD025020.

REFERENCES

(1). Roskoski R (2012) ERK1/2 MAP kinases: Structure, function, and regulation. Pharmacol. Res 66, 105–143. [PubMed: 22569528]

(2). Meloche SJ, and Pouysségur J (2007) The ERK1/2 mitogen-activated protein kinase pathway as a master regulator of the G1- to S-phase transition. Oncogene 26, 3227–3239. [PubMed: 17496918]

(3). Davies H, Bignell GR, Cox C, Stephens P, Edkins S, Clegg S, Teague J, Woffendin H, Garnett MJ, Bottomley W, Davis N, Dicks E, Ewing R, Floyd Y, Gray K, Hall S, Hawes R, Hughes J, Kosmidou V, Menzies A, Mould C, Parker A, Stevens C, Watt S, Hooper S, Wilson R, Jayatilake H, Gusterson BA, Cooper C, Shipley J, Hargrave D, Pritchard-Jones K, Maitland N, Chenevix-Trench G, Riggins GJ, Bigner DD, Palmieri G, Cossu A, Flanagan A, Nicholson A, Ho J, Leung SY, Yuen ST, Weber BL, Seigler HF, Darrow TL, Paterson H, Marais R, Marshall CJ, Wooster R, Stratton MR, and Futreal PA (2002) Mutations of the BRAF gene in human cancer. Nature 417, 949–954. [PubMed: 12068308]

(4). Montagut C, and Settleman J (2009) Targeting the RAF–MEK–ERK pathway in cancer therapy. Cancer Lett. 283, 125–134. [PubMed: 19217204]

(5). Jenkins RW, and Fisher DE (2020) Treatment of advanced melanoma in 2020 and beyond. J. Invest. Dermatol, 31257–31254.

(6). Karoulia Z, Gavathiotis E, and Poulikakos PI (2017) New perspectives for targeting Raf kinase in human cancer. Nat. Rev. Cancer 17, 676–691. [PubMed: 28984291]

(7). Kidger AM, Sipthorp J, and Cook SJ (2018) ERK1/2 inhibitors: New weapons to inhibit the RAS-regulated RAF-MEK1/2-ERK1/2 pathway. Pharmacol. Ther 187, 45–60. [PubMed: 29454854]

(8). Morris EJ, Jha S, Restaino CR, Dayananth P, Zhu H, Cooper A, Carr D, Deng Y, Jin W, Black S, Long B, Liu J, Dinunzio E, Windsor W, Zhang R, Zhao S, Angagaw MH, Pinheiro EM, Desai J, Xiao L, Shipps G, Hruza A, Wang J, Kelly J, Paliwal S, Gao X, Babu BS, Zhu L, Daublain P, Zhang L , Lutterbach BA, Pelletier MR, Philippar U, Siliphaivanh P, Witter D, Kirschmeier P, Bishop WR, Hicklin D, Gilliland DG , Jayaraman L, Zawel L, Fawell S, and Samatar AA (2013) Discovery of a novel ERK inhibitor with activity in models of acquired resistance to BRAF and MEK inhibitors. Cancer Discovery 3, 742–750. [PubMed: 23614898]

(9). Aronov AM, Tang Q, Martinez-Botella G, Bemis GW, Cao J, Chen G, Ewing NP, Ford PJ, Germann UA, Green J, Hale MR, Jacobs M, Janetka JW, Maltais F, Markland W, Namchuk MN, Nanthakumar S, Poondru S, Straub J, ter Haar E, and Xie X (2009) Structure guided design of potent and selective pyrimidylpyrrole inhibitors of extracellular signal-regulated kinase (ERK) using conformational control. J. Med. Chem 52, 6362–6368. [PubMed: 19827834]

(10). Hatzivassiliou G, Liu B, O'Brien C, Spoerke JM, Hoeflich KP, Haverty PM, Soriano R, Forrest WF, Heldens S, Chen H , Toy K, Ha C, Zhou W, Song K, Friedman LS, Amler LC, Hampton GM, Moffat J, Belvin M, and Lackner MR (2012) ERK inhibition overcomes acquired resistance to MEK inhibitors. Mol. Cancer Ther 11, 1143–1154. [PubMed: 22402123]

(11). Zhang F, Strand A, Robbins D, Cobb MH, and Goldsmith EJ (1994) Atomic structure of the MAP kinase ERK2 at 2.3 A resolution. Nature 367, 704–711. [PubMed: 8107865]

(12). Canagarajah BJ, Khokhlatchev A, Cobb MH, and Goldsmith EJ (1997) Activation mechanism of the MAP kinase ERK2 by dual phosphorylation. Cell 90, 859–869. [PubMed: 9298898]

(13). Kornev AP, and Taylor SS (2010) Defining the conserved internal architecture of a protein kinase. Biochim. Biophys. Acta, Proteins Proteomics 1804, 440–444.

(14). Huse M, and Kuriyan J (2002) The conformational plasticity of protein kinases. Cell 109, 275–282. [PubMed: 12015977]

(15). Xiao Y, Lee T, Latham MP, Warner LR, Tanimoto A, Pardi A, and Ahn NG (2014) Phosphorylation releases constraints to domain motion in ERK2. Proc. Natl. Acad. Sci. U. S. A 111, 2506–2511. [PubMed: 24550275]

(16). Xiao Y, Liddle JC, Pardi A, and Ahn NG (2015) Dynamics of protein kinases: Insights from nuclear magnetic resonance. Acc. Chem. Res 48, 1106–1114. [PubMed: 25803188]

(17). Baldwin AJ, and Kay LE (2009) NMR spectroscopy brings invisible protein states into focus. Nat. Chem. Biol 5, 808–814. [PubMed: 19841630]

(18). Eisenmesser EZ, Millet O, Labeikovsky W, Korzhnev DM , Wolf-Watz M, Bosco D, Skalicky JJ, Kay LE, and Kern D (2005) Intrinsic dynamics of an enzyme underlies catalysis. Nature 438, 117–121. [PubMed: 16267559]

(19). Zhang J, Shapiro P, and Pozharski E (2012) Structure of extracellular signal-regulated kinase 2 in complex with ATP and ADP. Acta Crystallogr., Sect. F: Struct. Biol. Cryst. Commun 68, 1434–1439.

(20). Pegram LM, Liddle JC, Xiao Y, Hoh M, Rudolph J, Iverson DB, Vigers GP, Smith D, Zhang H, Wang W, Moffat JG, and Ahn NG (2019) Activation loop dynamics are controlled by conformation-selective inhibitors of ERK2. Proc. Natl. Acad. Sci. U. S. A 116, 15463–15468. [PubMed: 31311868]

(21). Hoofnagle AN, Resing KA, Goldsmith EJ, and Ahn NG (2001) Changes in protein conformational mobility upon activation of extracellular regulated protein kinase-2 as detected by hydrogen exchange. Proc. Natl. Acad. Sci. U. S. A 98, 956–961. [PubMed: 11158577]

(22). Lee T, Hoofnagle AN, Resing KA, and Ahn NG (2005) Hydrogen exchange solvent protection by an ATP analogue reveals conformational changes in ERK2 upon activation. J. Mol. Biol 353, 600–612. [PubMed: 16185715]

(23). Rudolph J, Xiao Y, Pardi A, and Ahn NG (2015) Slow inhibition and conformation selective properties of extracellular signal-regulated kinase 1 and 2 inhibitors. Biochemistry 54, 22–31. [PubMed: 25350931]

(24). Horovitz A, Serrano L, Avron B, Bycroft M, and Fersht AR (1990) Strength and co-operativity of contributions of surface salt bridges to protein stability. J. Mol. Biol 216, 1031–1044. [PubMed: 2266554]

(25). Xiao Y, Warner LR, Latham MP, Ahn NG, and Pardi A (2015) Structure-based assignment of Ile, Leu and Val methyl groups in the active and inactive forms of the mitogen-activated kinase extracellular signal-regulated kinase 2. Biochemistry 54, 4307–4319. [PubMed: 26132046]

(26). Tugarinov V, and Kay LE (2004) An Isotope Labeling Strategy for Methyl TROSY Spectroscopy. J. Biomol. NMR 28, 165–172. [PubMed: 14755160]

(27). Mansour SJ, Candia JM, Matsuura JE, Manning MC, and Ahn NG (1996) Interdependent domains controlling the enzymatic activity of mitogen-activated protein kinase kinase 1. Biochemistry 35, 15529–15536. [PubMed: 8952507]

(28). Shapiro PS, Vaisberg E, Hunt AJ, Tolwinski NS, Whalen AM, McIntosh JR, and Ahn NG (1998) Activation of the MKK/ERK pathway during somatic cell mitosis: direct interactions of active ERK with kinetochores and regulation of the mitotic 3F3/2 phosphoantigen. J. Cell Biol 142, 1533–1545. [PubMed: 9744882]

(29). Resing KA, and Ahn NG (1997) Protein phosphorylation analysis by electrospray ionization-mass spectrometry. Methods Enzymol. 283, 29–44. [PubMed: 9251009]

(30). Delaglio F, Grzesiek S, Vuister GW, Zhu G, Pfeifer J, and Bax A (1995) NMRPipe: A multidimensional spectral processing system based on UNIX pipes. J. Biomol. NMR 6, 277–293. [PubMed: 8520220]

(31). Tugarinov V, and Kay LE (2003) Ile, Leu, and Val methyl assignments of the 723-residue malate synthase G using a new labeling strategy and novel NMR methods. J. Am. Chem. Soc 125, 13868–13878. [PubMed: 14599227]

(32). Vranken WF, Boucher W, Stevens TJ, Fogh RH, Pajon A, Llinas M, Ulrich EL, Markley JL, Ionides J, and Laue ED (2005) The CCPN data model for NMR spectroscopy: Development of a software pipeline. Proteins: Struct., Funct., Genet 59, 687–696. [PubMed: 15815974]

(33). Hansen DF, Yang D, Feng H, Zhou Z, Wiesner S, Bai Y, and Kay LE (2007) An exchange-free measure of 15N transverse relaxation: An NMR spectroscopy application to the study of a folding intermediate with pervasive chemical exchange. J. Am. Chem. Soc 129, 11468–11479. [PubMed: 17722922]

(34). Korzhnev DM, Kloiber K, and Kay LE (2004) Multiple-quantum relaxation dispersion NMR spectroscopy probing millisecond time-scale dynamics in proteins: Theory and application. J. Am. Chem. Soc 126, 7320–7329. [PubMed: 15186169]

(35). Palmer AG (2004) NMR characterization of the dynamics of biomacromolecules. Chem. Rev 104, 3623–3640. [PubMed: 15303831]

(36). Choy WY, Zhou Z, Bai Y, and Kay LE (2005) An 15N NMR spin relaxation dispersion study of the folding of a pair of engineered mutants of apocytochrome b562. J. Am. Chem. Soc 127, 5066–5072. [PubMed: 15810841]

(37). Sours KM, Xiao Y, and Ahn NG (2014) Extracellular signal-regulated kinase 2 is activated by the enhancement of hinge flexibility. J. Mol. Biol 426, 1925–1935. [PubMed: 24534729]

(38). Tong M, Pelton JG, Gill ML, Zhang W, Picart F, and Seeliger MA (2017) Survey of solution dynamics in Src kinase reveals allosteric cross talk between the ligand binding and regulatory sites. Nat. Commun 8, 2160. [PubMed: 29255153]

(39). Roser P, Weisner J, Simard JR, Rauh D, and Drescher M (2018) Direct monitoring of the conformational equilibria of the activation loop in the mitogen-activated protein kinase p38c. Chem. Commun 54, 12057–12060.

(40). Pucheta-Martinez E, Saladino G, Morando MA, Martinez-Torrecuadrada J, Lelli M, Sutto L, D'Amelio N, and Gervasio FL (2016) An allosteric cross-talk between the activation loop and the ATP binding site regulates the activation of Src kinase. Sci. Rep 6, 24235. [PubMed: 27063862]

(41). Meng Y, Pond MP, and Roux B (2017) Tyrosine kinase activation and conformational flexibility: Lessons from Src-family tyrosine kinases. Acc. Chem. Res 50, 1193–1201. [PubMed: 28426203]

(42). Sultan MM, Kiss G, and Pande VS (2018) Towards simple kinetic models of functional dynamics for a kinase subfamily. Nat. Chem 10, 903–909. [PubMed: 29988151]

(43). Jonniya NA, Sk MF, and Kar P (2019) Investigating phosphorylation-induced conformational changes in WNK1 kinase by molecular dynamics simulations. ACS Omega 4, 17404–17416. [PubMed: 31656913]

(44). Lopez ED, Burastero O, Arcon JP, Defelipe LA, Ahn NG, Marti MA, and Turjanski AG (2020) Kinase activation by small conformational changes. J. Chem. Inf. Model. 60, 821–832. [PubMed: 31714778]

(45). Kumar GS, Clarkson MW, Kunze MBA, Granata D, Wand AJ, Lindorff-Larsen K, Page R, and Peti W (2018) Dynamic activation and regulation of the mitogen-activated protein kinase p38. Proc. Natl. Acad. Sci. U. S. A 115, 4655–4660. [PubMed: 29666261]

(46). Lake EW, Muretta JM, Thompson AR, Rasmussen DM, Majumdar A, Faber EB, Ruff EF, Thomas DD, and Levinson NM (2018) Quantitative conformational profiling of kinase inhibitors reveals origins of selectivity for Aurora kinase activation states. Proc. Natl. Acad. Sci. U. S. A 115, E11894–E11903. [PubMed: 30518564]

(47). Gilburt JAH, Sarkar H, Sheldrake P, Blagg J, Ying L, and Dodson CA (2017) Dynamic equilibrium of the Aurora A kinase activation loop revealed by single-molecule spectroscopy. Angew. Chem., Int. Ed 56, 11409–11414.

(48). Piserchio A, Warthaka M, Kaoud TS, Callaway K, Dalby KN, and Ghose R (2017) Local destabilization, rigid body, and fuzzy docking facilitate the phosphorylation of the transcription factor Ets-1 by the mitogen-activated protein kinase ERK2. Proc. Natl. Acad. Sci. U. S. A 114, E6287–E6296. [PubMed: 28716922]

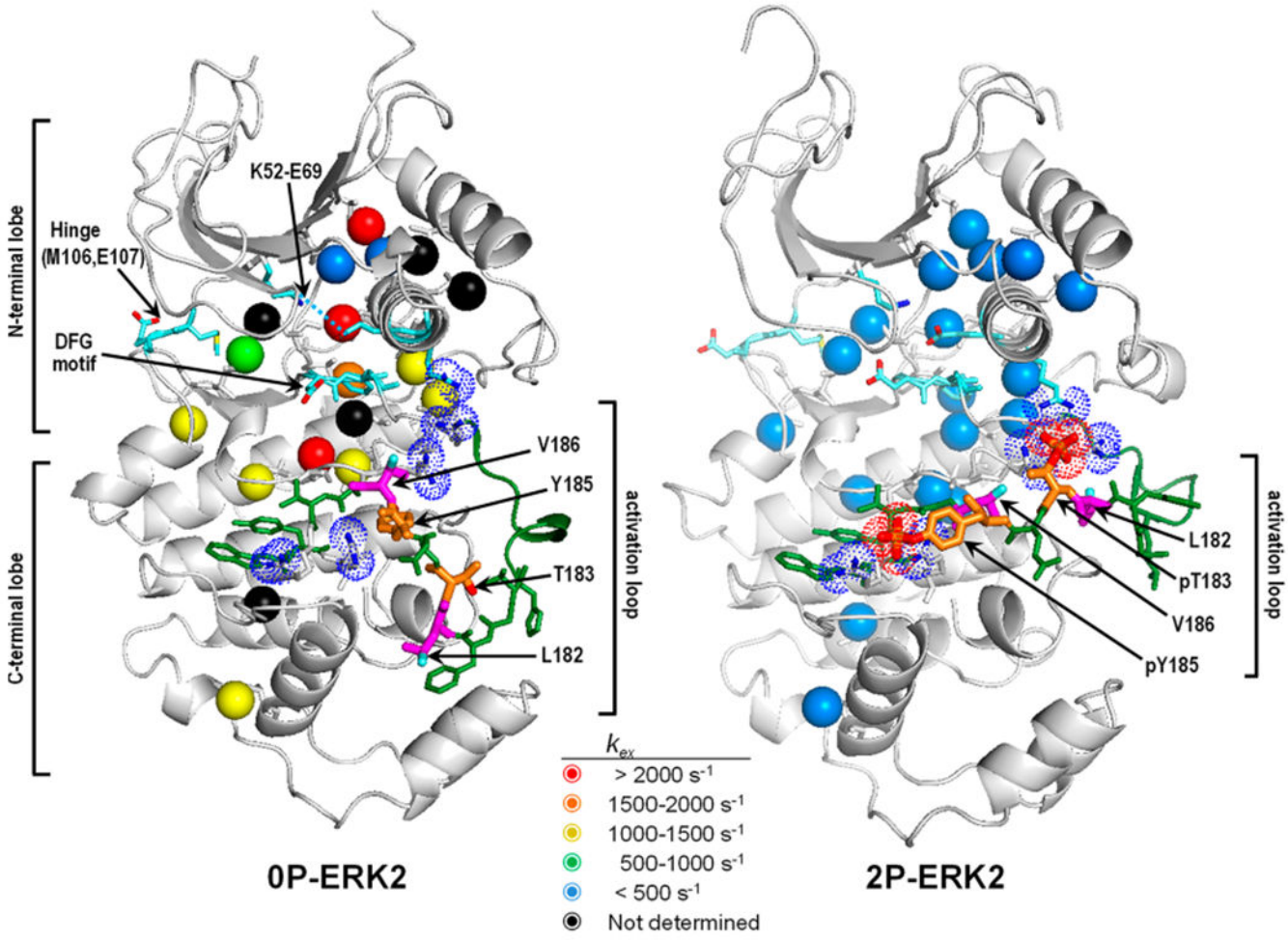

Figure 1.

Activation of ERK2 by phosphorylation forms a phosphate–Arg salt bridge network and introduces a slow global conformational exchange process. X-ray structures of inactive, unphosphorylated (0P) ERK2 (left, Protein Data Bank entry 5UMO) and active, dual-phosphorylated (2P) ERK2 (right, Protein Data Bank entry 2ERK), showing the locations of methyl probes in the kinase core that converge to a single slow exchange rate as reported by regression of the Carver–Richards formulation to CPMG relaxation–dispersion data. The activation loop (green) undergoes a large conformational rearrangement upon phosphorylation, where residues T183 and Y185 (orange) gain negative charge (red dots) and form salt bridges with positively charged Arg residues (blue dots). NMR resonances from residues L182 and V186 (magenta) are assigned in this study and examined as probes of activation loop motions. Residues that participate in the active site are colored cyan.

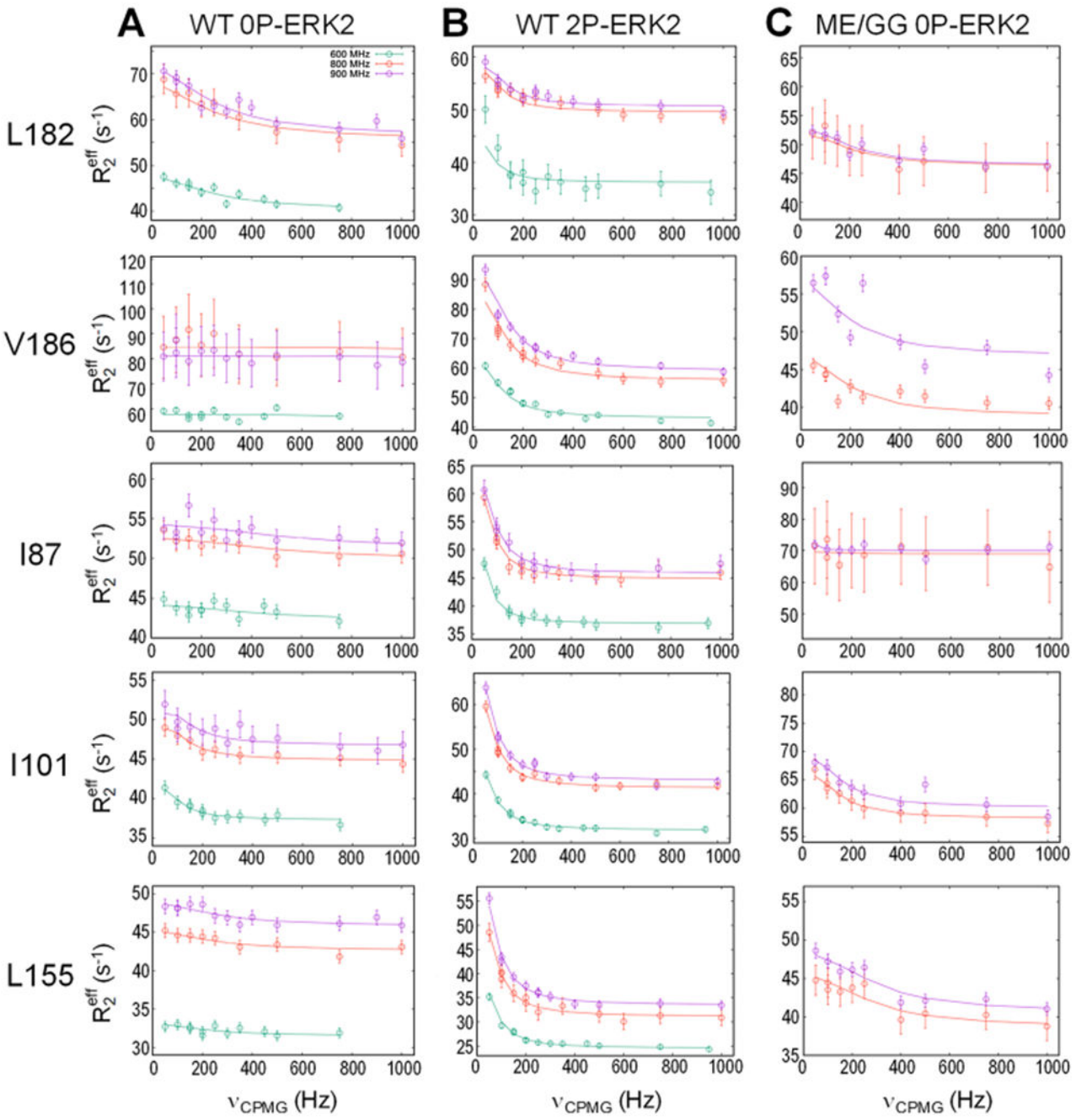

Figure 2.

Activation loop residues undergo slow conformational exchange following dual phosphorylation of WT ERK2 or mutation of the hinge region. CPMG relaxation–dispersion (RD) plots show changes in dynamics of [*methyl*-^{13}C]ILV residues in the activation loop (L182 and V186), similar to residues previously found to report slow global motions within the kinase core (e.g., I87, I101, and L155). Data collected at 600, 800, and 900 MHz are colored green, red, and purple, respectively. (A) RD of the activation loop and representative methyls in WT 0P-ERK2 report fast and uncorrelated exchange rates. (B) Each residue

shows a slower exchange rate and a greatly increased R_{ex} in WT 2P-ERK2. (C) Partial release of constraints to allow conformational exchange in the hinge mutation, $M_{106}E_{107}$/$G_{106}G_{107}$, is seen in core residues of 0P-ERK2 as well as the activation loop residues.

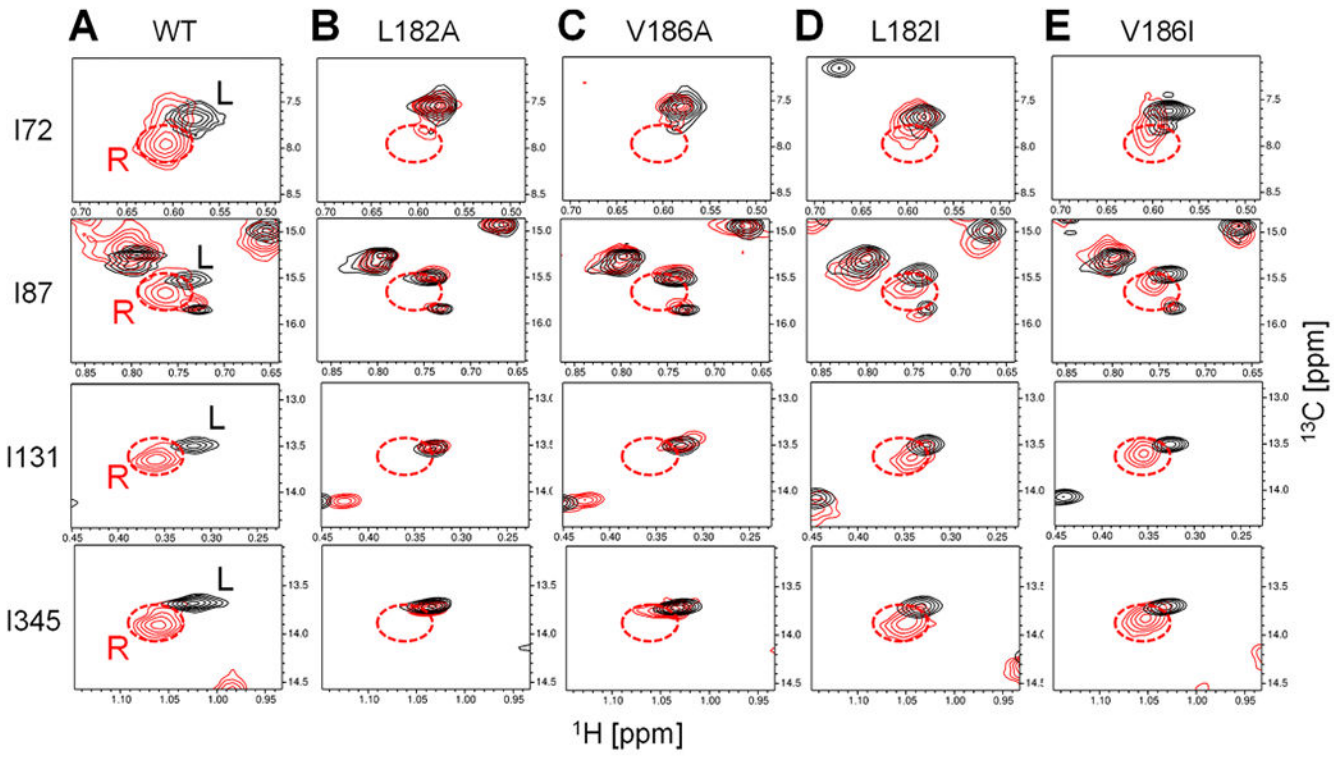

Figure 3.

Methyl peaks reveal changes in the chemical exchange of core residues following mutations at the activation loop. Shown are two-dimensional ^{13}C–^{1}H HMQC spectra of methyl peaks in 0P-ERK2 (black) and 2P-ERK2 (red) for representative core residues that report global motions following phosphorylation. (A) Peaks in WT 0P-ERK2 correspond to one conformer state (“L”), while 2P-ERK2 shifts to a new state (“R”) in equilibrium with the L state (L:R ratio of approximately 20:80). Activation loop mutations (B) L182A and (C) V186A disrupt the shift to the R state in 2P-ERK2. Conservative activation loop mutations (D) L182I and (E) V186I mostly preserve the shift to the R state. Variations in some residues can be observed in L182I, as shown in Figure S4.

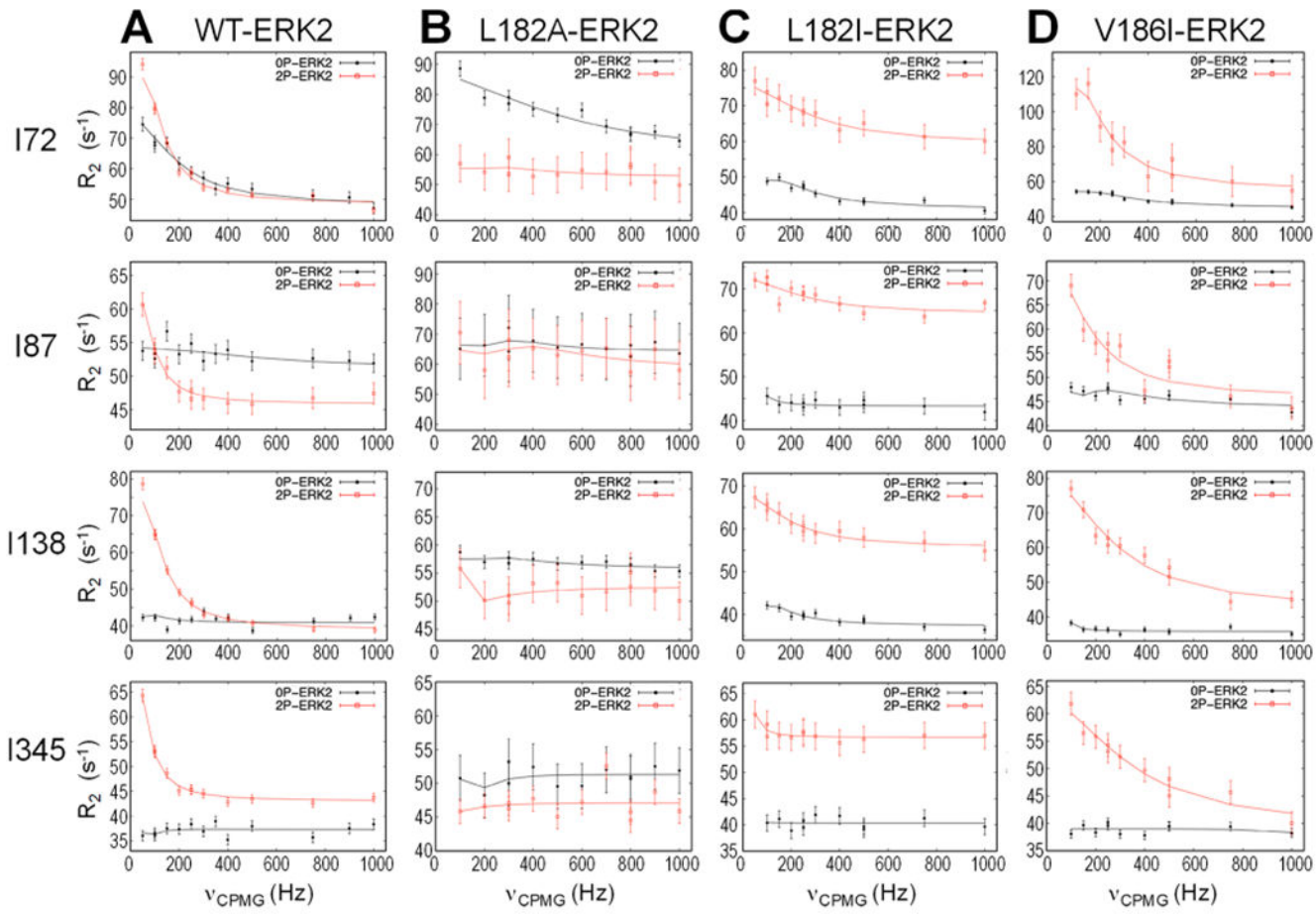

Figure 4.

CPMG relaxation–dispersion plots report changes in chemical exchange of core residues by mutations at the activation loop. CPMG relaxation–dispersion (RD) plots of data collected at 900 MHz for 0P-ERK2 (black) and 2P-ERK2 (red). Changes in dynamics of core residues seen in (A) WT ERK2 following phosphorylation appear (B) fully blocked by mutation L182A. Dynamics are (C) partially blocked in L182I and (D) preserved in V186I, but with a faster rate, k_{ex}. The results reveal coupling between motions of residues in the activation loop and kinase core. Additional examples are shown in Figure S5.